LONDON, METEOROLOGICAL OFFICE.
Met.O.15 Internal Report No.78

The quantitative use of Landsat imagery in cumulus studies.

03330889 551.501.776 551.507.362.2 FH5B

(279)

METEOROLOGICAL OFFICE
London Road, Bracknell, Berks.

MET.O.15 INTERNAL REPORT

No. 78

THE QUANTITATIVE USE OF LANDSAT IMAGERY IN CUMULUS STUDIES

by S.D.Rudman

March 1989

Cloud Physics Branch (Met.O.15)

Summary

The results of an initial study of Landsat Thematic Mapper imagery of a cumulus field are presented. The Thematic Mapper is described briefly and three techniques of quantitative data analysis are discussed: a calculation of the size distribution; a measure of the nearest-neighbour distance and estimates of cloud top height using a thermal window channel. Comparisons are made with other available data recorded during the satellite overpass and in the published literature.

Introduction

The linear dimensions of cumulus clouds are between 100s of metres and 10s of kilometres. For studies of fields of cumulus a spatial resolution of the order of magnitude of 10m is needed to examine cumulus in detail (Shenk and Salomonson (1972)) and a large sample of clouds must be in view to build accurate statistics of the field. These are required for progress in parametrisations of the radiative properties and the heat, water and mass transport of cumulus fields for use in numerical models of the atmosphere. These statistics will also deepen insight into the possible mechanisms of the mutual interaction of groups of clouds.

Conventional meteorological satellites have a large field of view but their resolution elements tend to be of size ≈1km and so are unsuitable for examining all but the largest clouds. Conversely, photographs from aircraft such as those made by Plank (1969) or Hozumi et al. (1982) achieve the spatial resolution but can only provide data on a few clouds and require corrections for perspective effects.

The Thematic Mapper (TM) instrument flown on satellites Landsat 4 and 5 has provided images in seven spectral bands at a nominal 30m resolution,each image being recorded in 25s and so encompassing an area 185km by 185km. The thermal channel has made the calculation of cloud top temperatures and therefore heights possible.

The SPOT satellite, launched in February 1986 has an instrument with a maximum resolution of 10m but suffers from the disadvantage of a swath width of only 117km and no thermal channel.

Thematic Mapper Description

The Thematic Mapper is a complex whiskbroom* scanner drawing on concepts and technology developed for the four-band Multispectral Scanners (MSS) flown on Landsats 1,2 and 3. Its spatial, radiometric and spectral resolutions are however much higher than those of MSS. Landsats 4 and 5 are in near-circular orbits of period 99 minutes and inclination 98.2°. This results in a sun-synchronous orbit in which the equator crossing time is set to 0940 GMT and the 50N crossing time over the UK is then 1020-1030 GMT. In this orbit each descending path is covered every 16 days but the path repetition sequence means that coastal areas of the UK may be imaged up to a handful of times a week. Currently (1988) only Landsat 5's TM is operationally used.

The ground cell element and scene size mentioned in the introduction result from the satellite's nominal altitude of 705km. Panoramic distortion or "perspective errors" occurring at maximum viewing angles are corrected for at the ground station by reference to attitude and altitude data received from the spacecraft support system.

The spectral bands have been listed in Table 1 together with other summary information; bands four and six have so far been investigated. Band four in the near infrared gives a uniform low reflectance for the ocean and lies in the spectral region where variable water vapour absorption and Rayleigh scattering are both small, whereas band six is the thermal channel. Band 5 has not yet been examined but may prove a better source of near infrared data than band 4 because it is subject to less Rayleigh scattering than band 4.

Images of Europe are received as part of ESA's Earthnet program at two ground stations: Kiruna in Sweden and Fucino in Italy. A full TM scene consists of approximately 270 Mbytes of data and occupies three 6250 bpi magnetic tapes. These may be purchased from the National Remote Sensing Centre in Farnborough, who also have

* **A whiskbroom scanner** employs an oscillating mirror which enables a single detector to make an across-track scan. The image is built up as the physical motion of the spacecraft moves this scan along track. A pushbroom scanner, on the other hand, uses a solid-state linear array of detectors which are able to take in the whole width of a scan at one go and therefore only require the spacecraft movement to allow an image to be formed.

an interactive image processing system for public use. A national archive of images is kept at NRSC but its usefulness in cloud physics is limited since most archived images are chosen for their lack of cloud.

Table One

Performance Data for the Thematic Mapper with the Multispectral Scanner of Landsats 1 through 3 as a Comparison

	Thematic Mapper			*Multispectral Scanner*		
	No.	Wavelength interval (μm)	Radiometric sensitivity (%)[a]	No.	Wavelength interval (μm)	Radiometric sensitivity (%)[a]
Spectral band designation	1	0.45– 0.52	0.40 0.65	4	0.5– 0.6	0.57
	2	0.52– 0.60	0.35 0.57	5	0.6– 0.7	0.57
	3	0.63– 0.69	0.43 0.57	6	0.7– 0.8	0.65
	4	0.76– 0.90	0.25 0.33	7	0.8– 1.1	0.70
	5	1.55– 1.75	0.60 1.68		Landsat 3 only:	
	6	10.4 –12.5	0.5 K	8	10.4–12.6	1.4 K
	7	2.08–2.35	2.00			
Ground-projected IFOV size	30 m × 30 m for bands 1–5 and 7 120 m × 120 m for band 6			76 m × 76 m for bands 4–7 234 m × 234 m for band 8[b]		
Data rate	83×10^6 bps			15×10^6 bps		
Quantization levels	256			64		
Interband registration	0.1 pixel			0.25 pixel		
Long-term scan stability	0.5 pixel			1.5 pixel		
Nominal equatorial crossing time	0930 hours local			0930 hours local		
Altitude	705 km			919 km		
Earth coverage	16-day period			18-day period		
Weight	325 kg			53 kg 4-band, 65 kg 5-band		
Size	0.9 m × 0.9 m × 1.8 m			0.35 m × 0.4 m × 0.9 m		
Power	250 W			42 W		

[a]The radiometric sensitivities are the noise-equivalent reflectance differences (temperature differences in the 10.4–12.6-μm band) expressed as percentages. For the Thematic Mapper the values in the right-hand column are worst-case estimates.
[b]Landsat 3 only.

Test Image

The techniques described in this report were devised and tested using a subimage from a Landsat 4 scene from the NRSC archive. The scene covered the English Channel south of Portsmouth (Landsat World Reference System location 202/25) and was recorded on 19/01/83. The synoptic situation was dominated by an anticyclone situated to the west of Ireland which was drawing cold air from the north over central England and southwards over the relatively warm Channel towards France. A field of fair-weather cumulus formed north of the Cherbourg peninsula and grew as they moved southwards. The subimage chosen was square and of dimensions 1024 pixels (30.72km x 30.72km); its top left corner had coordinates TL 2363 4712 in the full scene. It was chosen

because the cloud field appeared relatively homogeneous (the clouds at the south end were not appreciably bigger than those at the north end) and seemed to contain reasonably mature fair-weather cumulus. The subimage contained 126 clouds of effective diameter greater than 500m.

Measuring Cloud Cover

The proportion of cloudy picture elements in a band four image may be simply determined by setting a reflectance threshold and counting the pixels whose near-infrared radiance is above this. Given the high sensor resolution of TM, a bimodal histogram of pixel intensity is expected because pixels should be almost always cloudy or clear. This would lead to a well-defined cloud cover and sharp cloud edges in the image. Neither the sharp edgees nor the bimodal distribution have been observed in Landsat band 4 or band 6. To illustrate this point consider the contrast-stretched band 4 image in figure 1. As the intensity threshold is increased from the lowest pixel intensity in the image, the cloud cover fraction decreases continuously from unity to zero as shown in figure 2. This result was in agreement with the work of Wielicki and Welch (1986) who studied this effect in Landsat MSS images of cumulus fields over Southern Louisiana and the Western Atlantic. Their main explanation for this phenomenon was the variability of cloud reflectance so that there were areas of low reflectance which may be taken as ocean by a simple threshold scheme. Neglecting this argument of Wielicki and Welch and assuming a high-contrast cloud edge, atmospheric scattering would 'smear out' the view of such a small-scale feature when viewed from the top of the atmosphere and the edge would appear less well defined.

Since the cloud cover is a strong function of intensity threshold it is obviously important to choose the correct threshold. The following method was used to try to identify the correct value of cloud cover for the section of scene under consideration. It seeks to reduce this decision of where the cloud-ocean boundary lies on the reflectance grading to a decision of choosing what is and what is not a cloud. Ths was done by choosing an auxilliary subimage of identical dimensions as the main subimage described above but located further north where clouds were just beginning to form. It contained the smallest objects that an analyst judged to be clouds. These smallest clouds tend to have much lower peak reflectances than larger clouds and thus if the intensity threshold is set around their average

reflectance the larger clouds should be accurately defined. Deciding on this 'average reflectance' is not difficult because the smallest clouds are only a few pixels across and therefore do not show as clear a reflectance gradient across them. The result of this is that these clouds either are or are not counted in the cloud cover fraction; larger clouds are defined by more pixels and therefore have opportunity to show variable reflectance and can then only partly be counted for cloud cover. This means that for the smallest clouds the graph of cloud cover against threshold is most step-like.

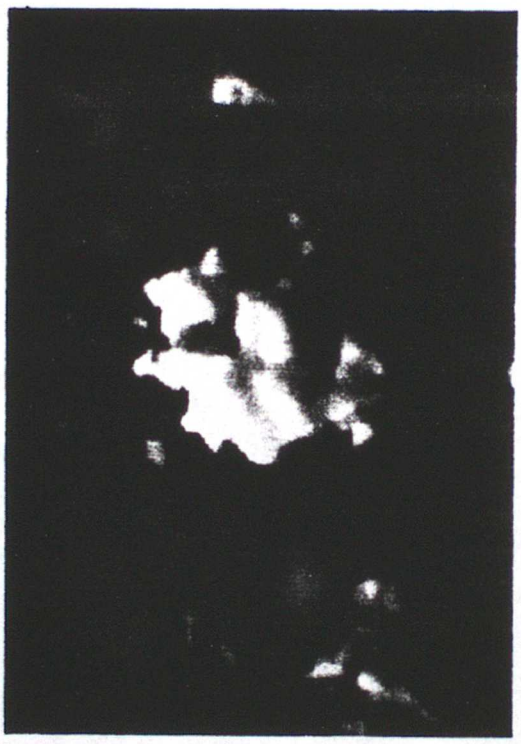

Figure 1 A band 4 view of a cloud approximately 2100m across

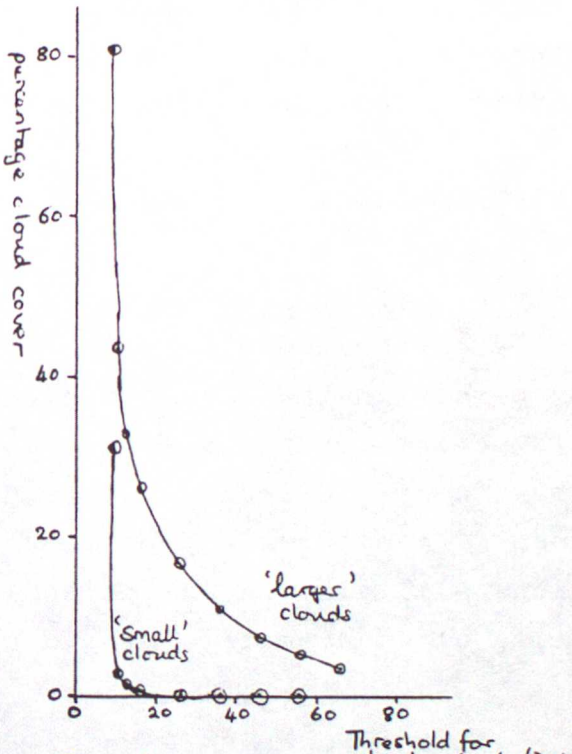

Figure 2
The effect of threshold for cloud on the cloud cover

Once a cloud cover was determined for band four reflectance, a temperature threshold was set for band six (thermal) by altering this threshold until the band six and band four cloud covers were the same. This ensures a degree of consistency between the two bands but a comparison of this threshold with one determined independently using only band six would be worthwhile. If it is assumed that cloud edge pixels represent cloud base temperatures the temperature threshold for cloud is the cloud base temperature and this was in approximate agreement with that calculated from the nearest tephigram. It was found that many 'clouds' of only a few pixels area in band four did not feature at all in band six because of this band's lower resolution (120m x 120m).

A commonly used method of cloud detection in satellite images originated with Coakley and Bretherton (1982). The mean and standard deviation for each group of four pixels in the thermal band scene are calculated. Standard deviation is plotted against mean thermal digital number and the points of low standard deviation represent the surface or the temperature of a well defined cloud layer. The cloud cover fraction in other pixels is determined by assuming that their radiance is a linear combination of the cloudy and clear radiances weighted by the cloud fraction. This method is unsuitable for cumulus fields because 100% cloudy pixels on a single cloud will have very different brightness temperatures and thus this scheme is of no use in identifying cloud in these circumstances.

Size Distributions

Having defined the cloudy pixels, an individual cloud area A may be easily determined given a rule for defining connectivity between cloudy pixels in the same cloud. Four-connectivity was usually used; this is satisfied when a pixel has a cloudy next-neighbour in either the image x or y direction. If eight-connectivity is selected then the presence of a cloudy neighbouring pixel in one of the four diagonal positions will also be sufficient for connectivity.This enables an effective cloud diameter D_{eff} to be calculated through the relation:

$$D_{eff} = \sqrt{4A/pi}$$

Despite the non-circularity of the observed cloud plans D_{eff} was used as a measure of cloud linear dimension. This was because of its simplicity and to enable comparison with the cloud statistics reported by other workers (eg Plank and Hozumi et al).

The program WKIMAG was written to calculate the areas, centroids and other measures of cloud images. Its automatic operation represented a major saving of effort over the performance of the measurements by hand. An automatic analysis of the band 4 subimage defined above was compared with subjective/objective estimates of cloud centroid and area for the clouds of area greater than 16 pixels in one quadrant of the subimage. Although slight differences between the automatic and hand procedures meant that the two lists of clouds and their areas and centroids could not be exactly the same, the hundred clouds which were common to both lists had identical areas and the centroids were within the error expected of the subjective

analysis scheme. The automatic system cost around eighty COSMOS units whereas the hand scheme would have required around eight days of work on the GEMS system to cover a similar image area. The method of image analysis used is described in the appendix. At this point it is sufficient to regard it as a black box producing a table giving cloud area, centroid and sums of various moments of pixel position for each distinct cloud observed.

From the area list a histogram of the frequency distribution of Deff may be calculated. Examples for the fair weather cumulus subimage described under 'Test Image' and for another subimage of the same size and band but observed over the North Sea are shown in fig 3. The frequency for a class with Deff limits x x+dx represents the probability of finding a cloud in 1km^2 area with the class width normalised to 1km in Deff. Each class contained at least 20 clouds. To achieve this required only a small class width for small Deff and in this region the outline of the histogram was then drawn as a continuous curve. The resulting differences in class boundaries cause the apparent discrepancy between the two histograms of this author.

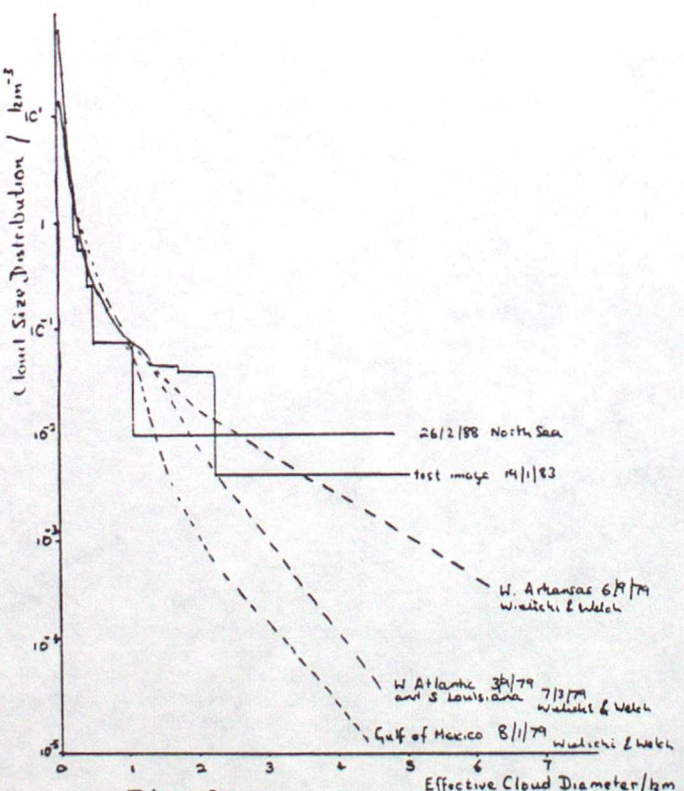

Fig 3a Cloud size distributions compared with the data of Wielicki and Welch, Plank, and Hozumi et al.

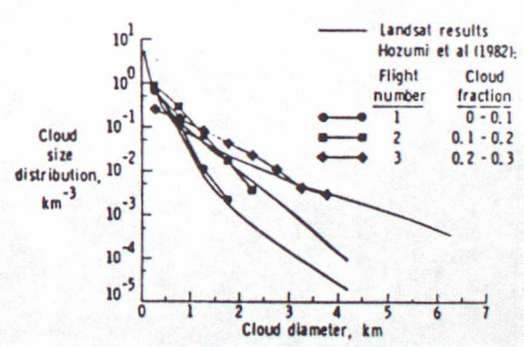

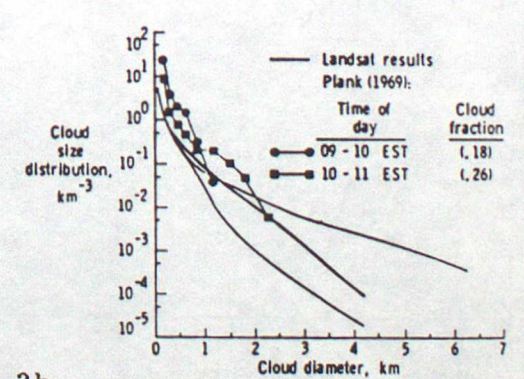

Fig 3b

Comparison of the Landsat-derived cloud size distributions in Fig. 11 with previous results derived from subjective analyses of aircraft photographs. Figure 12a compares the current results to aircraft flights south of Japan in February 1974 and 1975 reported by Hozumi et al., (1982). Figure 12b compares the current results to aircraft flights over the Florida Peninsula in August and September 1957 reported by Plank (1969).

Figure 3 also shows a comparison of the Met Office data and that of other authors, who use different functions in curve fitting to the

Deff histogram. Plank (1969), Wielicki and Welch (1986), Hozumi et al (1982) and Joseph (1985) fit to a simple exponential function exp(-Deff/constant) whereas Lopez (1976) prefers fitting to a lognormal function. The exponential function is appropriate to a cloud field whose members have a Deff which increases linearly with time and who have a distribution of ages which is uniform. The lognormal function is appropriate to clouds whose rate of increase of Deff is proportional to their size; Lopez calls this a law of 'proportional growth'.

Fig 3a shows good agreement between the results of Wielicki and Welch and those of the author. Fig 3b is reproduced from Wielicki and Welch and compares their curves with those of Hozumi et al and Plank. All four sets of observations show data of similar form. The median and modal cloud sizes are the smallest observable scale in each case and are of the order of 50m.

Fig 3c

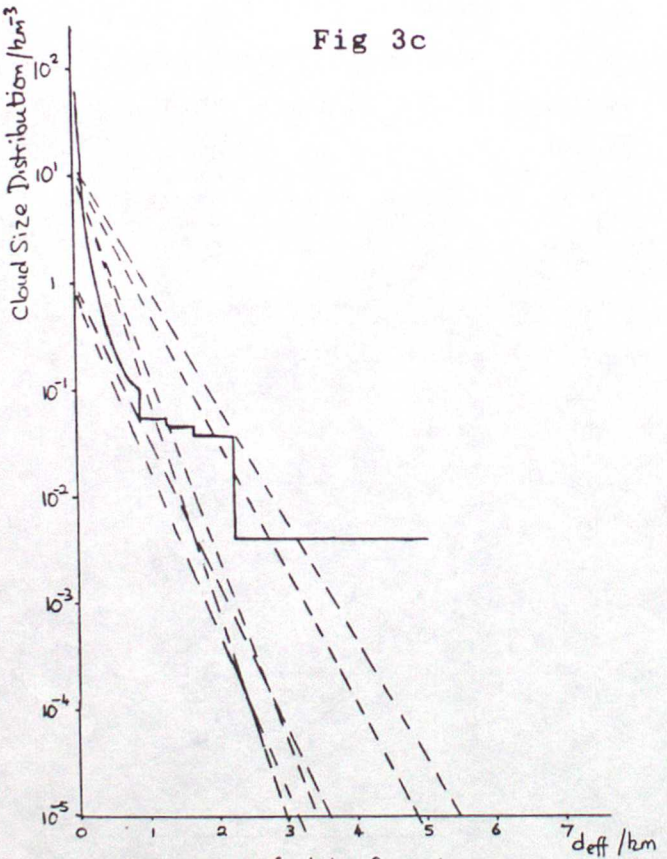

Comparison of data from test image with best-fit size distributions of Joseph.

Fig 3d

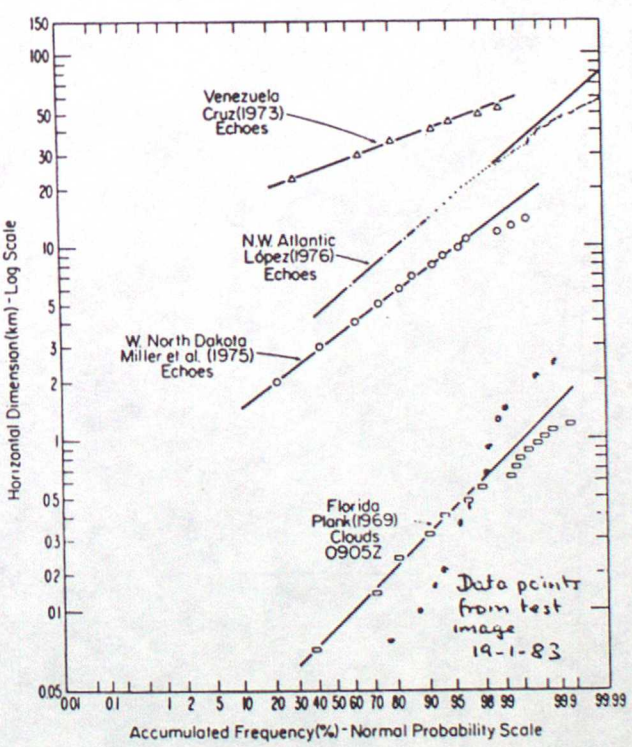

Accumulated frequency distributions of cloud and echo horizontal dimension. The straight lines correspond to the log-normal distributions that best fit the different data sets.

Figures 3c shows a comparison between the author's results and the best fit curves of Joseph. The fit of Joseph's exponential decrease of frequency with Deff seems to be a very simplistic model for the frequency distribution observed by Wielicki and Welch, Plank, Hozumi et al and the author. The observed data show an exponential

behaviour only for D_{eff} greater than 2km. For D_{eff} less than 2km the observed frequency distribution decreases at a rate greater than an exponential.

In figure 3d the author's data is drawn on a diagram from a paper by Lopez in which Lopez plotted cloud D_{eff} calculated from the radar and photogrammetric measurements of himself, Plank and other workers. Lopez proposed the use of a lognormal distribution for cloud D_{eff}, rooting it in a law of 'proportional effects'. The results from the present experiments were plotted on this diagram. It can be seen that the present results trace what is approximately a straight line and are therefore approximate Lopez lognormal distribution. Although all the data on Lopez plot are lognormally distributed, there are large differences in observational scale and it is not obvious that all of Lopez data is relevant to this study of small cumulus.

Perhaps a greater body of data, especially one containing more observations of clouds of D_{eff} greater than 1.3km, is needed before a firm conclusion can be reached concerning the most appropriate fit.

Nearest Neighbour Distributions

In order to characterise separation of clouds in the field, the distances between clouds and their nearest neighbours were examined. The first measure of the cloud separation used was the shortest distance between two cloud centroids. For every cloud identified by the image analysis program a distance was calculated from its centroid to that of each of the other clouds on the list. The smallest separation between the first cloud and one of the other clouds on the list was attributed to the first cloud as its Nearest-Neighbour Distance (NND). In an attempt to characterise the distance between the cloud edges, half of D_{eff} for a given cloud and half of D_{eff} for its nearest neighbour were removed from the first cloud's NND. If the clouds were circular in plan the new distance d_{sep} would represent the distance between the cloud's edges. This crude measure of separation was used as the distributor in a frequency distribution . In order to begin to explore the influence of cloud size on d_{sep} distributions, a diameter threshold was set which eliminated all clouds with D_{eff} below it from the calculations. For each value of the area threshold the mean d_{sep} over the distribution was calculated and fig 4 shows this mean plotted against area threshold. When the threshold was reduced towards zero, thus tending to include all clouds, the mean separation

between circular clouds tended towards zero. That this should be so is an indication that the following situation dominates the mean d_{sep}: rings of diameter D_{eff} around the centroids of numerous very small clouds are located extremely close to the D_{eff} ring drawn around the cloud centroid of their nearest neighbour. If they represent something like cumulus fractus formed from cloud decay or cloud elements formed in the updraught of a 'mother' cloud this close separation seems reasonable.

As the threshold was increased the mean d_{sep} increased rapidly until d_{sep} became almost constant with D_{eff} threshold. The levelling off occurred when the threshold was about 0.6km and the mean d_{sep} was 0.55±0.03km. A further increase in the threshold reduced the number of clouds contributing to the mean d_{sep} and hence the standard error of the mean increased.

Figure 4
Cloud separation as a function of minimum area allowed in analysis

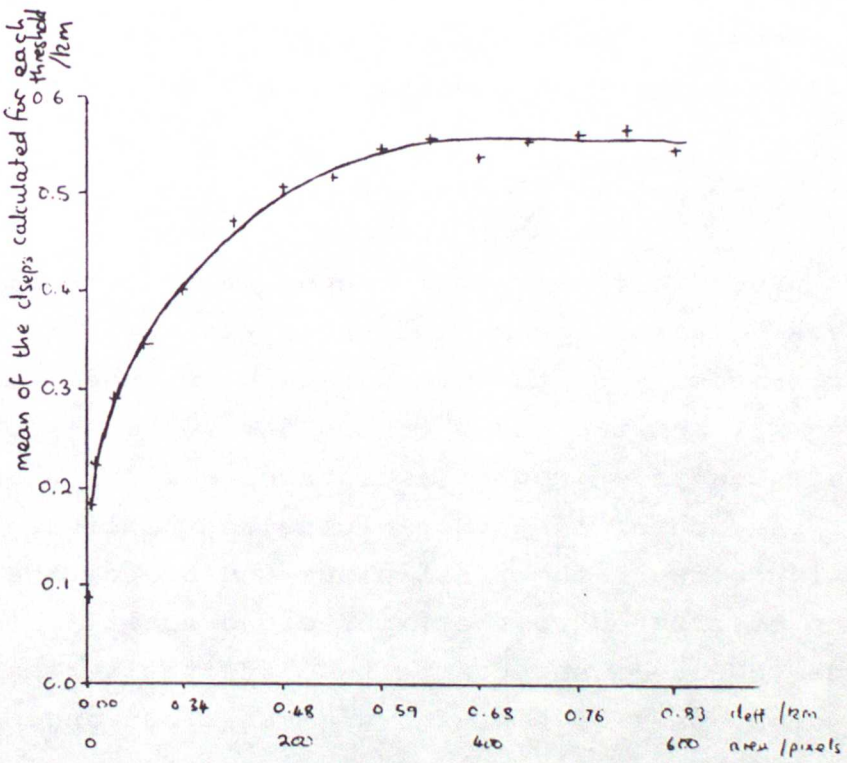

These results may be interpreted within the framework of ideas expounded by Hill which were derived from a numerical model of a cumulus field. In the updraughts of a large number of small boundary layer circulations small cloud elements form. As latent heat is released on condensation, further impulse is provided to the updraught strength. The increased interaction between neighbouring circulations result in the merging and strengthening of some cells and the annihilation of others. Some new small cloud elements are spawned in the large updraughts of the merged cloud 'clumps'. This leads to a

population of fewer,larger, more widely separated clouds than before which are ringed by growing small cloud elements. From the results in the figure it would appear that on average the 'larger' clouds are those with an effective diameter greater than 0.6km. The small-cloud picture appears to be dominated at this stage in the field's development by those ringing larger clouds. The smaller clouds representing some of the decaying initial circulations do not appear to have a significant impact on the d_{sep} average.

It may be argued that the curve of figure 4 could be explained by a systematic change of cloud shape with D_{eff} while the cloud NND remains constant. An examination of the image suggests that the departures from circularity in cloud shape are rather random and that the variation of the spacing is more plausible. It also seems unlikely that edge effects arising from the square boundary of the 36km x 36km assembled image are important when d_{sep} is less than 1 km.

In order to perform these calculations rapidly program CUBIT was written to compute a list of d_{sep}s for each of four area thresholds supplied as JCL control cards. Two subroutines are available to calculate the separation; NNDCALC calculates NND and NNDCALC2 obtains d_{sep}. The table produced is machinable to enable further analysis of the values

Vertical Dimensions of clouds

The infrared window channel (band 6) was used to estimate cloud top height. EOSAT calibration constants were used to calculate spectral radiance from the digital number on tape. Owing to differences in ground processing between ESA and EOSAT these constants will not be exactly appropriate to the ESA-processed data available in Europe but the lack of good ESA calibration data requires their use.

From spectral radiance, temperature may be calculated from the Planck function if the attenuating and scattering effect of the atmosphere is ignored.The result is a map of cloud top temperature with ground cell resolution 120m x 120m and thermal resolution of about 0.5°c. If the cloud base temperature and pressure are known the cloud top pressure and height may be calculated if it is assumed the the cloud top air rose along a saturated adiabat from cloud base. The software developed to perform these calculations uses the band 4 sliced image as a template to determine the cloud edge; band 4's

resolution enables a band 6 pixel cloudiness to be specified to a precision of half an okta. The maps of cloud top temperature are not as yet output directly but rather summary information in the form of cloud-mean, cloud-minimum or cloud-maximum radiances, temperatures or heights are given. It is also possible to obtain cloud volumes from the program.

The size of retrieval errors is not easily predicted and may vary greatly from case to case. A large source of systematic error is incurred in neglecting the effect of the atmosphere on the signal received; the magnitude of this will vary from day to day. Water vapour absorption alone may cause errors of up to 10°c (Li and McDonnell (1988)) but in the absence of fronts or strong sea surface temperature gradients it seems likely that an offset to all temperatures derived within a scene would correct for the presence of the atmosphere. The use of EOSAT calibration constants may also contribute to the systematic error; this error may be temperature dependent and would not be corrected by a uniform offset; this error is at present unknown (A. Wilson (NERC), private communication). Digitization errors are another source of error; the radiometric resolution of the thermal channel is only 0.5°c in the cloud-top temperature range and so the retrieved temperatures will suffer from random digitization errors of ±0.25°c.

Figure 5 is a scatter diagram of each cloud's minimum pixel temperature against the cloud's area for a 512 by 1024 extract from a scene recorded on 26/02/88. The cloud-minimum temperature decreases for bigger clouds. Large-area clouds would be expected to be tall (and cold-topped) clouds and very small clouds may be so tenuous that some radiation from the warm sea surface may be transmitted through the cloud. The difference between the sea-surface temperature from the corrected Barnes radiometer measurement and that from Landsat-5 is around 0.6°c and so no offset to the Landsat temperatures seems necessary.The aircraft-measured sounding suggests an average cloud-top temperature between -5°c and -10°c; this is midway between the two extremes of minimum brightness-temperature measured. The 'average cloud-top temperature' derived from the temperature and dew point profile characterises an ensemble of different clouds, each of whose cloud-tops is not an obviously identifiable level unless a strong inversion flattens the tops. Depending on the shape of the cloud a different definition of 'average cloud-top temperature' is appropriate in analysing the different pixel temperatures measured across a cloud

field. Taking the minimum temperature measured on each cloud as representing the cloud top is acceptable for fairly flat-topped clouds or columnar thermals but may give a slightly cold bias for a hypothetical cloud of triangular cross-section (figure 6). Bearing in mind these difficulties, figure 5 shows reasonable agreement between in-situ and Thematic Mapper measurements.

Conclusions

A detailed analysis of a Landsat scene containing cumulus gives a large amount of information about the cloud field but its reduction to a few summary distributions or statistics is not straightforward conceptually, unless the irregularity of the cloud shape is ignored by considering circular-plan clouds of the same area and centroid as the real cloud.

Cloud size distributions made using the above assumption compare well with published data except the best fit lines to Joseph's results. In this case it is the form of the best fit lines rather than the fit constants which seem to cause the discrepancy.

In quantifying the nearest neighbour distance between clouds d_{sep} was developed as a measure. It was found that the ensemble mean of d_{sep} increases as the area threshold for inclusion in the analysis increases until the effective cloud diameter is about 0.6km. Above this threshold the mean d_{sep} remains around 0.55km. This may represent a stage in cloud growth when the merging and separating of clouds described by Hill ceases. These values of d_{sep} and D_{eff} may be dependent on a number of parameters such as boundary layer depth and static stability.

The calculation of cloud top temperatures has shown to be feasible and the resolution in brightness temperature appears to be sufficient to specify cloud top heights to a precision of the order of 5% of the boundary layer depth. There are systematic errors involved which need to be calculated for each image before the temperature data is useful. This may be done by comparison with in-situ information from, for example, an aircraft or possibly by employing an atmospheric transmission model such as LOWTRAN.

Future work could make use of Landsat in studies of the transport properties of cumulus fields and may be of use in providing spatial structure data for modelling radiation transfer through broken cloud. A deeper understanding of the effect of sub-pixel sized clouds on the

performance of meteorological satellites will also require a source of high resolution imagery and TM imagery will be of value in this.

Figure 5

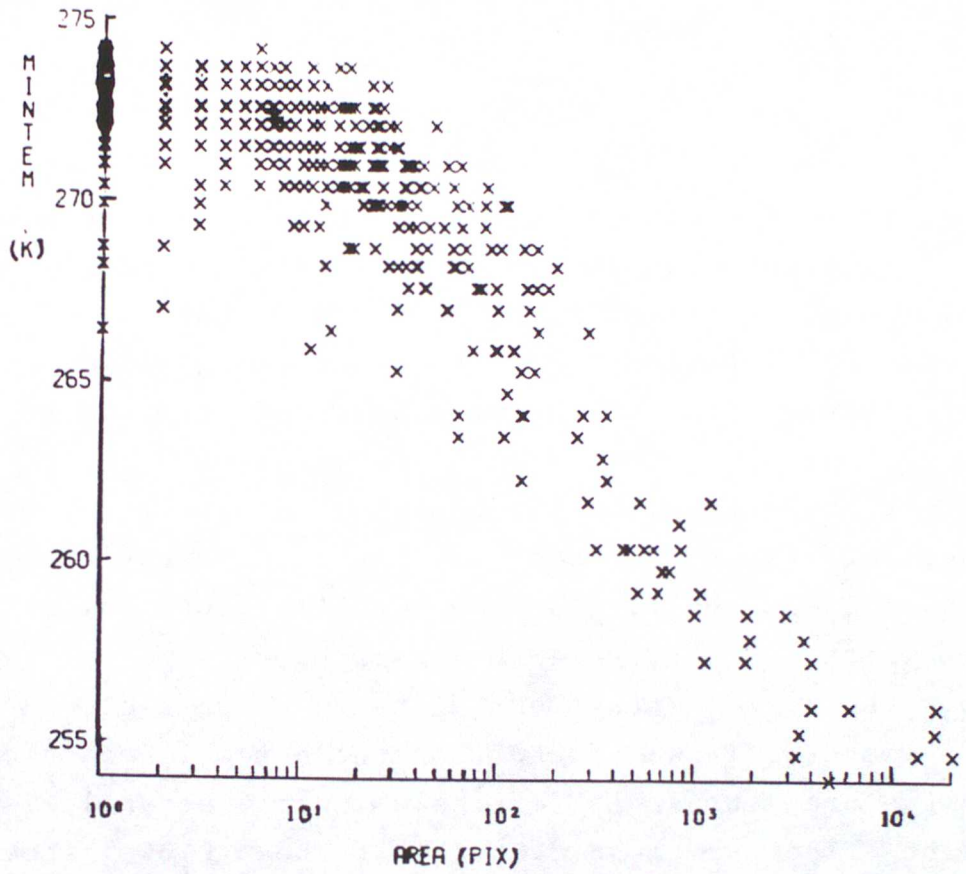

Minimum pixel temperature and cloud area for each cloud which is not edge occluded

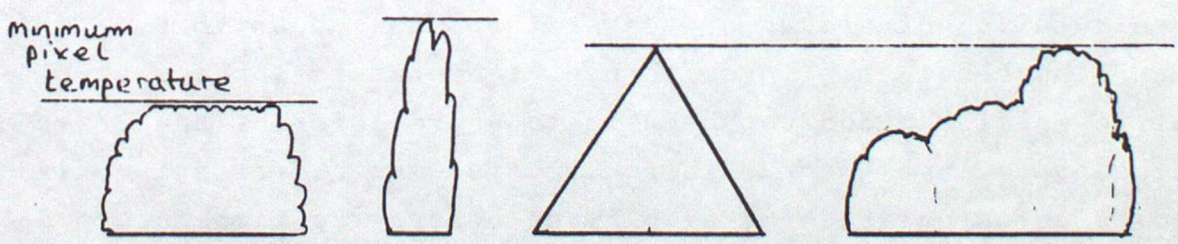

Figure 6 Cloud vertical cross section affects the representativeness of a cloud top measure such as minimum pixel temperature

Appendix: Image Processing Software

The batch processing schemes used for near-infrared and the thermal infrared are shown in figure 7. The input data is selected using an interactive GEMS machine and is dumped to tape as 512 x 512 pixel subimages (128 x 128 for the thermal channel). Core memory on COSMOS limits the maximum image size to 1024 pixels square and the assembly of the maximum of four subimages is performed by the program.

When processing band 6, JCL control cards allow the specification of different moments for output and either the minimum, maximum or mean of the quantities digital number, spectral radiance, brightness temperature or pressure for each cloud. If pressure is selected, then a further option of cloud area multiplied by the cloud thickness in mb is available. This is loosely termed 'volume' and is proportional to cloud mass.

Band 4 images are supplied to the program already sliced so that (pixel)=1 represents cloud and (pixel)=0 represents the ocean. Band 6 images are prepared so that every pixel of value greater (warmer) than a threshold is set to 0 and the pixels of lesser value are left unchanged. This is done in such a way as to leave a margin of band 6 data around most of the band 4 cloud images. If there is no band 6 data when the band 4 mask is superimposed on the thermal image and a cloud top mean is required, then the code -9555 is printed against that cloud. If more than 5% and less than 100% of the mask area is without band 6 data a code of -9999 is printed. These codes are generally only needed for clouds of only a few pixels in area.

References

Coakley, J.A and F.P.Bretherton 1982, J. Geophys. Res., 87, no. C7, 4917-4932

Joseph, J.H 1985, Adv. Space Res., 5, 213-216

Hozumi, K., Harimaya, T. and C. Magono 1982, J. Met Soc. Japan, 60 ,691-699

Li, Z.R. and M.J McDonnell 1988, Int. J. Rem. Sens., 9, 107-121

Lopez, R.E 1977, Mon. Wea. Rev., 105, 865-872

Plank, V.G. 1969, J Appl. Met., 8, 46-67

Shenk, W.E., and V.V. Salomonson 1972, J. Appl. Met., 11, 214-220

Wielicki, B.A and R.M. Welch 1986, J. Clim. Appl. Met., 25, 261-276

Figure 7 Processing Scheme for Landsat Imagery